Using the optical-klystron effect to increase and measure the intrinsic beam energy spread in free-electron-laser facilities

Eduard Prat,[1,*] Eugenio Ferrari,[2] Sven Reiche,[1] and Thomas Schietinger[1]
[1]*Paul Scherrer Institut, CH-5232 Villigen PSI, Switzerland*
[2]*Particle Accelerator Physics Laboratory, École Polytechnique Fédérale de Lausanne EPFL, CH-1015 Lausanne, Switzerland*
(Received 2 November 2016; published 10 April 2017)

We present a setup based on the optical klystron concept, consisting of two undulator modules separated by a magnetic chicane, that addresses two issues in free-electron-laser (FEL) facilities. On the one hand, it allows increasing the intrinsic energy spread of the beam at the source, which is useful to counteract the harmful microbunching instability. This represents an alternative method to the more conventional laser heater with the main advantage that no laser system is required. On the other hand, the setup can be used to reconstruct the initial beam energy spread, whose typical values in FEL injectors around 1 keV are very difficult to measure with standard procedures.

DOI: 10.1103/PhysRevAccelBeams.20.040702

I. INTRODUCTION

Free-electron lasers (FELs) are cutting-edge research tools in multiple scientific fields that allow the observation of matter with ultra-high spatial and time resolutions. Current x-ray FEL facilities generate coherent radiation with wavelengths down to the Angstrom level, peak powers of tens of gigawatts or more, and pulse durations of tens of femtoseconds and shorter [1–5].

In this article we propose a setup based on the optical klystron effect [6–10], consisting of two undulator modules and a magnetic chicane in between, as shown in Fig. 1, to increase and measure the intrinsic or uncorrelated energy spread of the electron beam. The setup may be utilized to address two important issues in FEL facilities: the increase of the intrinsic beam energy spread is useful to suppress the so-called microbunching instability via Landau damping [11–14], while the high-resolution measurement of the intrinsic beam energy spread of the electron source provides important information in view of the characterization and optimization of the source. From now on we will refer to the intrinsic beam energy spread simply as beam energy spread.

The high-brightness beams generated in FEL facilities are prone to suffer a microbunching instability, which, if not counteracted, deteriorates the electron beam quality such that only reduced FEL amplification occurs in the undulator beamline [11–14]. An effective way to suppress the microbunching instability is to increase the initial beam energy spread. This is normally achieved with a so-called *laser heater* [14,15]: at relatively low energy (on the order of 100 MeV) the beam is arranged to propagate along an undulator, in parallel with an optical laser beam, such that the interaction in the modulator causes an energy modulation of the electron beam. The laser heater is typically situated between the second and third dipole magnet of a dispersive chicane, which smears out the energy modulation, leading to an effective increase of the beam energy spread. An electron beam energy of about 100 MeV is convenient because, for standard undulator periods, the corresponding radiation wavelength is in the range of commercially available lasers. To mitigate the microbunching instability effectively, the laser heater should be placed before the beam is longitudinally compressed in the first bunch compressor of the facility. The effectiveness of the laser heater has been demonstrated experimentally at the Linac Coherent Light Source [16] and at the FERMI facility [17]. Most of the other present and future FEL projects plan to employ it, including the European XFEL [18] in Germany, PAL-XFEL in South Korea [19], and SwissFEL in Switzerland [20,21].

Alternative schemes to increase the beam energy spread without the use of a laser have been presented: using a superconducting undulator to induce quantum fluctuations [22], based on transverse-deflector rf structures [23], introducing longitudinal phase mixing to the electron beam in a magnetic chicane [24], and employing transverse-gradient undulators [25].

Here we explore the potential of the setup sketched in Fig. 1 to increase the beam energy spread in FEL facilities, as an alternative to the laser heater. The chicane converts the energy modulation created in the first undulator module into a bunching, which in turn gives rise to an enhanced increase of the energy modulation in the second undulator module.

*eduard.prat@psi.ch

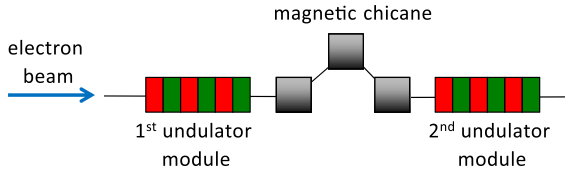

FIG. 1. Schematic layout of the proposed scheme for controlling and measuring the intrinsic energy spread of electron beams.

An important advantage of our proposal with respect to the laser heater is that it does not require any laser.

The setup can also be used to reconstruct with high resolution the initial beam energy spread by finding the chicane strength that maximizes the optical klystron effect. The initial beam energy spread has typical values around 1 keV or less, very challenging to measure with magnetic spectrometers, which in practice have a maximum resolution of a few keV for electron beams with energies on the order of 100 MeV or more [26]. Only a precise measurement makes it possible to tune the FEL injector parameters to achieve an optimum beam energy spread. The proposed method to measure the beam energy spread is similar to the one presented in Ref. [27], which also makes use of two undulator sections and a chicane, but requires a laser in addition.

We describe our scheme in more detail in Sec. II. In Sec. III we demonstrate the validity of our scheme with numerical simulations performed with the FEL code Genesis 1.3 [28] for parameters based on the SwissFEL design.

II. DESCRIPTION OF THE SCHEME

Figure 1 shows an illustration of the scheme based on the optical klystron, consisting of two undulator modules and a magnetic chicane in between. The length of our setup is similar to that of a laser heater, i.e., a few meters. In contrast to a laser heater, where the electron beam size has to match the laser mode size, our method does not require matching to any special optics at the undulator modules. Since the process relies on amplification through self-amplified spontaneous emission (SASE), however, having a small beam size will generally improve the method's efficiency, giving access to the desired final beam energy spread with shorter undulator modules. The installation of the setup upstream of the first bunch compressor of the FEL facility ensures that its large longitudinal dispersion (R_{56}) will eliminate microbunching and smear out the energy modulation generated in the undulators. From now on we will assume that the energy modulation generated after the second undulator module is equivalent to an increase of the beam energy spread.

A. Increase of the beam energy spread

The SASE process starts in the first undulator module, inducing an initial energy modulation to the electron beam. The R_{56} of the magnetic chicane in the optical klystron converts the energy modulation generated in the first undulator module into a density modulation (bunching), enabling a fast growth of the radiation power and the beam energy spread in the second undulator module. Without the chicane the undulator beamline required to increase the beam energy spread to a given level would be much longer—about a factor of three for the SwissFEL parameters, as we will see in Sec. III. Most importantly, the chicane gives the possibility to fine-tune the increase of the beam energy spread with the R_{56} of the chicane, equivalent to the variation of the laser power in the case of the laser heater [16,17]. Other options to control the beam energy spread in our setup are possible, but much less straightforward. For instance, the undulator length could be changed on a fine scale (on the order of a few cm) by opening the gap of certain undulator blocks or the beam optics or trajectory could be modified to attain a certain beam energy spread.

Our method is based on the SASE mechanism, which starts up from the electron shot noise and results in a spiky radiation profile. Therefore, the induced beam energy spread will not be constant along the longitudinal position of the bunch and will vary from shot to shot. However, due to the radiation slippage the induced beam energy spread is much more homogeneous than the SASE radiation profile itself, enough to mitigate the microbunching instability for the whole bunch. Although a laser is not required in our setup, it could still be added to improve the homogeneity of the beam energy spread along the bunch.

The induced beam energy spread due to the optical klystron effect is null when $R_{56} = 0$. With growing R_{56} the given energy modulation in the first undulator section converts to stronger bunching in the second stage, where the emission is more coherent, inducing a further energy modulation on a faster scale. The increase of the beam energy spread reaches a maximum at R_{56}^*, which we define as the R_{56} resulting in maximum gain of the optical klystron effect. For $R_{56} > R_{56}^*$ the beam is overbunched, leading to a reduction of the efficiency of the optical klystron effect and therefore of the final energy spread of the beam. From an operational point of view, operating at $R_{56} > R_{56}^*$ is not reasonable, since the same final beam energy spread can also be achieved with a smaller R_{56}.

The maximum achievable beam energy spread depends on the power gain of the optical klystron, which is inversely proportional to the ratio between the initial relative beam energy spread $\sigma_\delta = \sigma_E/E$ (where σ_E is the beam energy spread and E the mean energy of the beam) and the FEL parameter ρ [29]: for a given σ_δ, the power gain is higher for larger ρ, which is larger for higher beam quality (i.e., when the beam emittance and sizes are smaller and the current is higher) [9].

B. Measurement of the initial beam energy spread

The optimum chicane strength R_{56}^* for a maximum power gain of the optical klystron depends on the initial

energy spread of the beam but is quite insensitive to other beam parameters. According to one-dimensional (1D) theory [9]:

$$R_{56}^{*} \approx \frac{\lambda}{2\pi\sigma_{\delta}}, \tag{1}$$

where λ is the radiation wavelength. The above equation is valid when the energy modulation generated in the first undulator module is small compared to the initial beam energy spread, which is the case for the simulations presented here. For beams of extreme brightness with very low energy spreads, the length of the first undulator could be reduced to fulfill this condition.

Based on Eq. (1) it is possible to reconstruct the initial energy spread of the beam by finding the chicane strength that maximizes the optical klystron effect. This can easily be done by scanning the R_{56} of the chicane while measuring the resulting radiation power or the final beam energy spread—even without absolute measurements of these two quantities. The measurement of the output beam energy spread is usually done with a magnetic spectrometer, which is normally resolution limited to a few keV, while the radiation energy can readily be measured down to very low values (e.g., with a photodiode). Consequently, we suggest to reconstruct the initial beam energy spread by measuring the output radiation energy as a function of the chicane's R_{56}.

Three-dimensional (3D) effects will slightly modify Eq. (1). A more accurate reconstruction of the initial beam energy spread can be achieved by measuring the radiation power as a function of the chicane strength and comparing this curve with 3D simulations.

We note that our measurement method can be applied without any additional cost in the undulator beamline of an FEL facility if a magnetic chicane is available between two undulator sections. The latter condition is fulfilled for x-ray FEL facilities with a self-seeding chicane and for those facilities that envisage employing the optical klystron effect to reduce the saturation length, as in the case of SwissFEL [30].

C. Discussion on the radiation wavelength

Since our method is based on the SASE process, it works for a wide range of wavelengths. Its intrinsic self-tuning allows for any given beam energy and undulator parameters (period and length), while in the laser heater the seed laser has to match the undulator resonant wavelength, thereby limiting the range of beam energies and undulator parameters to be used. The wider operational range of our method allows us to work with radiation wavelengths for which the microbunching gain is negligible, at different locations of the facility with different beam energies, etc.

For given beam and undulator parameters, a longer wavelength is favorable since it corresponds to a higher undulator field, which in turn improves the coupling between the electron and photon beams, thereby increasing the radiation power and the induced beam energy spread. Therefore, the required undulator to achieve a certain beam energy spread will be shorter for a longer wavelength. However, the required R_{56} for the optical klystron configuration increases with the radiation wavelength [see Eq. (1)]. As a consequence, longer wavelengths require higher R_{56} and therefore stronger dipole magnets and/or longer magnetic chicanes. In summary, the radiation wavelength must be long enough to avoid too long undulators, but not too long such that the chicane parameters stay within reasonable limits. Furthermore, the wavelength should stay away from the range of wavelengths amplified by the microbunching instability.

Our method to measure or increase the beam energy spread also works if the electron beam has an energy chirp (a correlation between energy and longitudinal coordinate of the beam)—the different longitudinal slices with different energies will simply radiate at different wavelengths defined by their energies. At the center of the chicane there is a finite transverse dispersion, i.e., a correlation between the transverse coordinate and the energy of the electrons. Therefore, if the beam has an energy chirp at the chicane center, it will also have a correlation between the transverse and longitudinal coordinates. Consequently, a transverse collimator at this location would collimate the beam also longitudinally, allowing a local beam energy spread increase/measurement only for the beam slices passing through the collimator. A movable collimator could then be used to measure the beam energy spread as a function of the longitudinal position of the bunch. The function of the collimator could also be provided by a slotted foil [31]. We note that the beam would be compressed or decompressed due to its energy chirp and the chicane R_{56}, possibly affecting the microbunching gain along the accelerator.

III. NUMERICAL EXAMPLE FOR SWISSFEL

We consider the nominal beam parameters at the location of the laser heater of SwissFEL for a bunch charge of 200 pC [20,32]: the beam centroid energy is 150 MeV, the current profile is flat with a constant value of 20 A, and the normalized emittance is 200 nm. The beam energy spread is expected to be between 0.5 keV and 2 keV. Therefore, for the simulations presented here we will assume different initial beam energy spread values ranging between 0.5 and 2 keV. (All beam energy spread numbers throughout this work refer to rms values.) Concerning the beam optics, for both planes the initial β and α-functions are 10 m and 1, respectively. The incoming vertical optics is chosen to minimize the variation of the vertical beam size along the lattice when changing the chicane R_{56}. The simulations

presented in this section have been performed with Genesis 1.3. As an input we use an ideal beam for which the above-mentioned parameters are constant along the bunch.

We choose undulator modules with a period of 40 mm and a total length of 1.8 m each. Furthermore, we consider a planar undulator configuration with focusing only in the vertical plane. We note, however, that our scheme also works with helical undulators, which offer a higher electron-radiation coupling and are more convenient operationally for the beam optics because the undulator focusing in this case is symmetric in both transverse planes. The emission wavelength is set to 600 nm, corresponding to an rms undulator parameter of 1.256, and R^*_{56} values of 28.6 mm and 7.2 mm for initial beam energy spreads of 0.5 keV and 2 keV, respectively.

A magnetic chicane to achieve R_{56} values up to about 30 mm can be realized in a space of less than 1 m. For the simulations here we assume a chicane with three dipole magnets occupying in total 0.6 m: the first and the last dipole have a length of 0.1 m, the second dipole has a length of 0.2 m, and the drift between the magnets is 0.1 m. For our beam parameters, the required magnetic field to generate an R_{56} of 30 mm would be 1.5 T, which can be achieved with standard dipole magnets. Therefore, the whole setup fits into a length of about 4 m, similar to the space required for the laser heater of SwissFEL.

Figure 2 shows, for the case with an initial beam energy spread of 1 keV and an R_{56} of 10 mm, the bunching factor and the beam energy spread (averaged over the bunch length) along the system, together with the beam energy spread along the bunch for three different locations of the setup. The chicane's R_{56} increases the bunching from practically zero to about 0.05, which is fundamental to increase the radiation power and beam energy spread in the second undulator module. The final beam energy spread has a mean value of 11.4 keV, with an rms fluctuation along the bunch of 4.9 keV.

We have simulated the performance of our setup as a function of the chicane R_{56} for different initial beam energy spreads between 0.5 and 2 keV. The R_{56} is scanned between 0 and 36 mm in steps of 0.5 mm. For each case we run five simulations using different random seeds for the electrons' noise generation to take into account the shot-to-shot fluctuations intrinsic to the SASE process. Figure 3 shows the simulation results of the final beam energy spread and radiation energy at the end of the system as a function of the R_{56} for initial beam energy spreads of 0.5 and 2 keV. The error bars in this figure and the following ones account for the statistical shot-to-shot variations. The shot-to-shot fluctuations in output radiation energy and beam energy spread are around 4% and 2%, respectively. We observe that the final beam energy spread and radiation power follow a similar pattern and that both quantities reach their maxima at equivalent R^*_{56}.

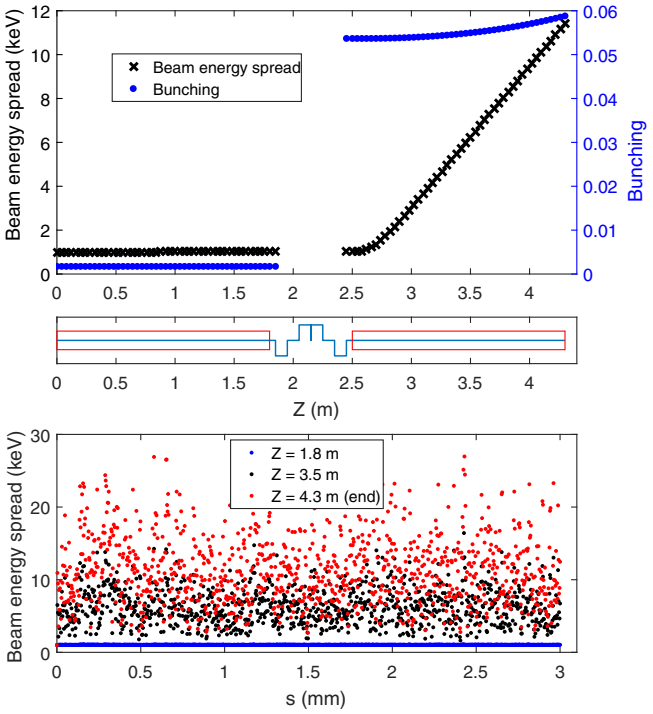

FIG. 2. Simulation results for an initial beam energy spread of 1 keV and a longitudinal dispersion of 10 mm. Top: average beam energy spread (black crosses, left axis) and bunching (blue dots, right axis) along the longitudinal position of the system. Bottom: beam energy spread along the longitudinal position of the bunch for three different locations: $Z = 1.8$ m (before the chicane), $Z = 3.50$ m, and $Z = 4.3$ m (end of the second undulator module).

A. Increase of the beam energy spread

The chicane's R_{56} can be used in a simple and efficient way to control the final beam energy spread on the rising edge of the curves plotted in Fig. 3. Figure 4 shows the

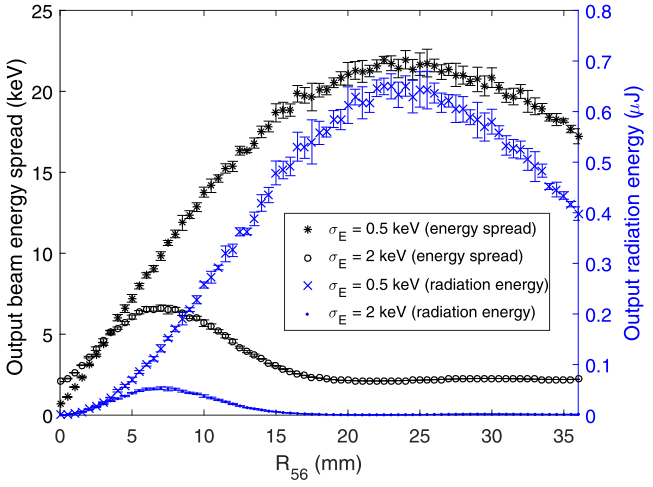

FIG. 3. Simulated induced beam energy spread (black, left axis) and radiation energy (blue, right axis) as a function of the chicane's R_{56} for initial beam energy spreads of 0.5 keV and 2 keV.

maximum achievable beam energy spread as a function of the incoming beam energy spread. We see that we can increase the beam energy spread to about 7 keV or more. This is sufficient in our case, considering that the laser heater of SwissFEL is expected to increase the beam energy spread up to a maximum of 7 keV, which is the highest tolerable beam energy spread before compression to avoid degrading the FEL performance of SwissFEL [21].

For the 1 keV case, our simulations indicate that, without taking advantage of the optical klystron effect, an effective undulator length of 12.5 m would be required to achieve the same maximum final beam energy spread (12.5 keV), about three times longer than in our proposed setup. This length could be reduced by employing an undulator with shorter period, e.g., a superconducting undulator, or by applying stronger focusing to the electron beam. In any case, as stated earlier, a solution without chicane would be much less favorable in terms of system tunability.

B. Measurement of the initial beam energy spread

In Fig. 3 we see the expected strong dependence of the R_{56}^{*} on the incoming energy spread of the beam. Our simulation results indicate that the R_{56}^{*} changes between about 7 mm and 24 mm for initial beam energy spreads varying between 2 keV and 0.5 keV. Figure 5 shows the reconstructed initial beam energy spread according to Eq. (1) as a function of the true initial beam energy spread. We determine the R_{56}^{*} by fitting a second-order polynomial function to the simulated curve describing the output properties (beam energy spread and radiation power) as a function of the R_{56} in a limited region around the maximum value. From Fig. 5 it is evident that equivalent reconstructed values are obtained when using the final beam energy spread or the radiation power for the measurement. The error bars shown in Fig. 5, which are below 0.1 keV, are dominated by the uncertainty of the second-order fit parameters due to shot-to-shot fluctuations. We also observe the presence of a systematic error on the reconstructed value in the form of a small underestimation when the initial beam energy spread is 2 keV, and an overestimation for beam energy spreads of 1 keV or less. This overestimation increases at smaller beam energy spreads, reaching 0.1 keV at an initial beam energy spread of 0.5 keV.

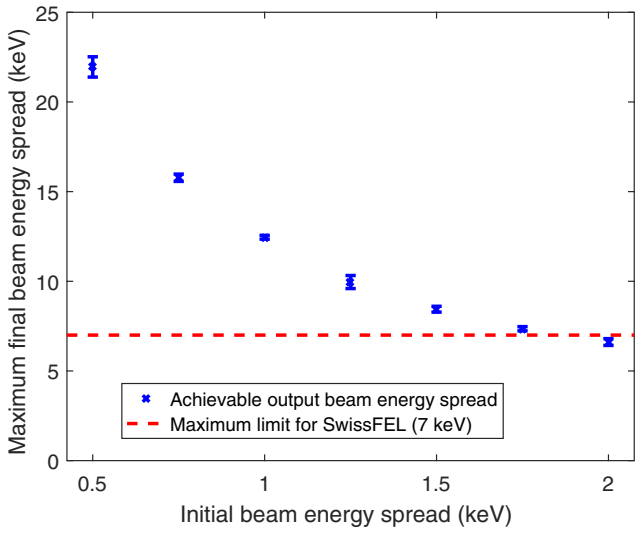

FIG. 4. Achievable beam energy spread as a function of the initial beam energy spread.

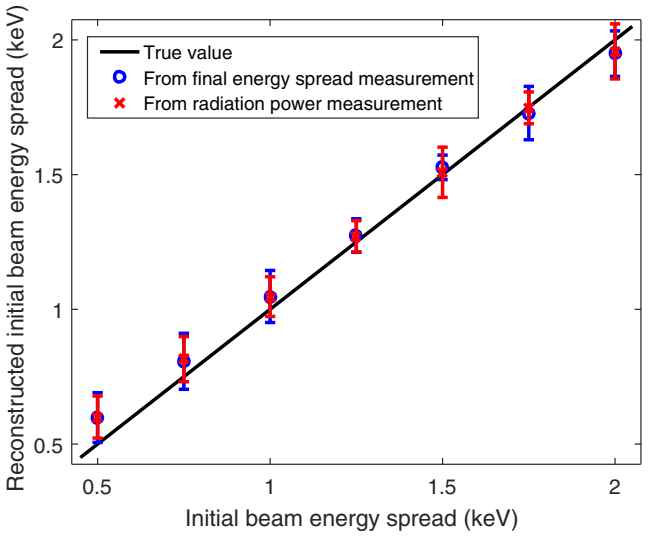

FIG. 5. Simulated reconstructed beam energy spread for different initial beam energy spreads.

As mentioned earlier, the resolution limitations of the final beam energy spread measurement lead us to recommend the reconstruction of the initial beam energy spread based on measurements of the radiation power as a function of the R_{56}. At SwissFEL, for instance, the beam energy spread measurement performed with a magnetic spectrometer has a resolution, due to finite beam size, of around 10 keV, while standard photodiodes can measure radiation energies of picojoules and below, with relative accuracy in the permille range. Considering that the shot-to-shot fluctuations are at the percent level, our diagnostics accuracy is more than sufficient to not add any significant error to the measurement of the initial beam energy spread.

Figure 6 shows the final beam energy spread and the square root of the radiation energy as a function of the R_{56} when the initial beam energy spread is 1 keV. The square root of the radiation energy is normalized to the maximum value of the final beam energy spread. The two curves are almost identical, as expected, given that the radiation power or energy is proportional to the square of the radiation field, which itself is proportional to the final energy spread of the beam. The small discrepancy at very low R_{56} can be explained by the fact that the beam has some finite energy spread even for very small values of R_{56}. The dependence provides an opportunity to calibrate with our setup the final

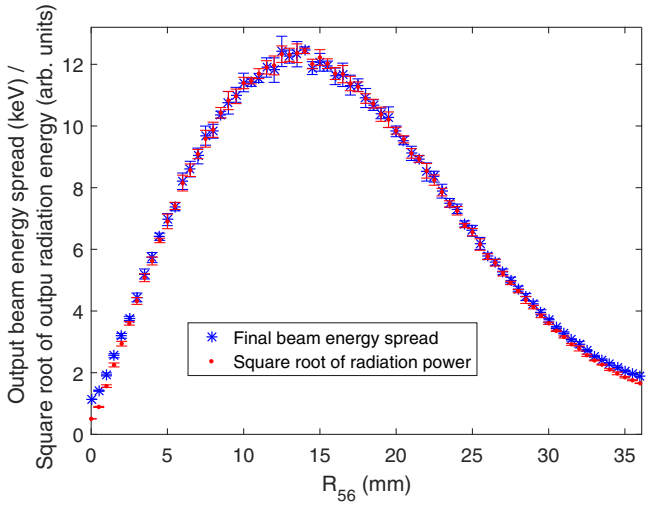

FIG. 6. Output beam energy spread and square root of the output radiation power as a function of the chicane's R_{56}.

beam energy spread by measuring the radiation energy with a photodiode, assuming that the output beam energy spread can be measured at least at its maximum value.

We have performed numerous additional simulations to assess the robustness of the method against beam parameter variations. Simulating the measurement procedure for five different beam currents between 10 and 30 A (in steps of 5 A) for an initial beam energy spread of 1 keV, we obtain an average value for the reconstructed beam energy spread of 1.05 keV and a standard deviation of 0.02 keV among the five measurements. Equivalent results are obtained when varying the normalized transverse emittance between 100 and 300 nm in steps of 50 nm. The deviation of the reconstructed beam energy spread for different currents or emittances (0.02 keV) is much smaller than the statistical error for a single case (up to 0.1 keV). We conclude that, within reasonable limits, changes in beam current and emittance have no significant effect on the reconstructed initial beam energy spread. Instead, the measurement errors appear to be dominated by the statistical uncertainty to obtain R_{56}^{*} and the systematic error arising from the shortcomings of the 1D theory. In a real experiment this last discrepancy could be reduced by comparing the measured values with 3D numerical simulations, obtained, e.g., with Genesis 1.3.

For illustration purposes, all previously presented results were obtained with an ideal beam distribution with uniform properties along the bunch. Nevertheless, the method still works for more realistic beams. We have tested the procedure for an electron beam obtained with the code ASTRA [33] for a realistic SwissFEL configuration: the method correctly reconstructs the average core energy spread of this beam, which is about 0.6–0.7 keV. As mentioned earlier, one could apply the procedure in conjunction with a collimator in the chicane to reconstruct the local beam energy spread for a certain longitudinal position along the electron bunch.

IV. CONCLUSION

We have presented a novel setup based on the optical klystron effect, consisting of two undulator modules and a chicane in between, that can be utilized both to increase and to measure the beam energy spread in FEL driving linacs. The increase of the beam energy spread is essential to suppress the microbunching instability in FEL facilities and is usually achieved with a laser heater. The setup presented here provides the same functionality without the need for a laser system, thereby evading all associated focusing and synchronization issues. The accurate measurement of the initial beam energy spread, usually too small to be measured with standard approaches based on magnetic spectrometers, is of great value when tuning the FEL injector for optimum performance.

ACKNOWLEDGMENTS

We are indebted Hans Braun for improving this work through fruitful discussions. We also thank Simona Bettoni for providing the particle distribution that we used as input for some of our simulations.

[1] P. Emma *et al.*, First lasing and operation of an ångstrom-wavelength free-electron laser, Nat. Photonics **4**, 641 (2010).
[2] T. Ishikawa *et al.*, A compact X-ray free-electron laser emitting in the sub-ångström region, Nat. Photonics **6**, 540 (2012).
[3] P. Emma *et al.*, Demonstration of self-seeding in a hard-X-ray free-electron laser, Nat. Photonics **6**, 693 (2012).
[4] E. Allaria *et al.*, Two-stage seeded soft-X-ray free-electron laser, Nat. Photonics **7**, 913 (2013).
[5] W. Ackermann *et al.*, Operation of a free-electron laser from the extreme ultraviolet to the water window, Nat. Photonics **1**, 336 (2007).
[6] N. A. Vinokurov and A. N. Skrinsky, BINP Report No. 77-59, 1977.
[7] P. Elleaume, Optical klystrons, J. Phys. Colloques **44**, C1-333 (1983).
[8] E. L. Saldin, E. A. Schneidmiller, and M. V. Yurkov, DESY Report No. 03-108, 2003.
[9] Y. Ding, P. Emma, Z. Huang, and V. Kumar, Optical klystron enhancement to self-amplified spontaneous emission free electron lasers, Phys. Rev. ST Accel. Beams **9**, 070702 (2006).
[10] G. Penco, E. Allaria, G. De Ninno, E. Ferrari, and L. Giannessi, Experimental Demonstration of Enhanced Self-Amplified Spontaneous Emission by an Optical Klystron, Phys. Rev. Lett. **114**, 013901 (2015).
[11] S. Heifets, G. Stupakov, and S. Krinsky, Coherent synchrotron radiation instability in a bunch compressor, Phys. Rev. ST Accel. Beams **5**, 064401 (2002).

[12] Z. Huang and K.-J. Kim, Formulas for coherent synchrotron radiation microbunching in a bunch compressor chicane, Phys. Rev. ST Accel. Beams **5**, 074401 (2002).
[13] E. L. Saldin, E. A. Schneidmiller, and M. V. Yurkov, Klystron instability of a relativistic electron beam in a bunch compressor, Nucl. Instrum. Methods Phys. Res., Sect. A **490**, 1 (2002).
[14] E. L. Saldin, E. A. Schneidmiller, and M. V. Yurkov, Longitudinal space charge-driven microbunching instability in the TESLA Test Facility linac, Nucl. Instrum. Methods Phys. Res., Sect. A **528**, 355 (2004).
[15] Z. Huang, M. Borland, P. Emma, J. Wu, C. Limborg, G. Stupakov, and J. Welch, Suppression of microbunching instability in the linac coherent light source, Phys. Rev. ST Accel. Beams **7**, 074401 (2004).
[16] Z. Huang *et al.*, Measurements of the linac coherent light source laser heater and its impact on the x-ray free-electron laser performance, Phys. Rev. ST Accel. Beams **13**, 020703 (2010).
[17] S. Spampinati *et al.*, Laser heater commissioning at an externally seeded free-electron laser, Phys. Rev. ST Accel. Beams **17**, 120705 (2014).
[18] M. Altarelli *et al.*, DESY Report No. 2006-097, 2007.
[19] T.-Y. Lee *et al.*, Design and physics issues of the PAL-XFEL, J. Korean Phys. Soc. **48**, 791 (2006).
[20] SwissFEL Conceptual Design Report, edited by R. Ganter, PSI Report No. 10-04, 2012.
[21] M. Pedrozzi, M. Calvi, B. D. Fell, R. Ischebeck, S. Reiche, N. Thompson, and C. Vicario, The laser heater system of SwissFEL, in *Proceedings of the 36th International Free-Electron Laser Conference, Basel, Switzerland, 2014* (JACoW, Geneva, 2015), p. 871.
[22] J. Arthur *et al.*, SLAC Report No. SLAC-R-593, 2002.
[23] C. Behrens, Z. Huang, and D. Xiang, Reversible electron beam heating for suppression of microbunching instabilities at free-electron lasers, Phys. Rev. ST Accel. Beams **15**, 022802 (2012).
[24] S. Di Mitri and S. Spampinati, Microbunching Instability Suppression via Electron-Magnetic-Phase Mixing, Phys. Rev. Lett. **112**, 134802 (2014).
[25] D. Huang, C. Feng, H. Deng, Q. Gu, and Z. Zhao, Transverse to longitudinal phase space coupling in an electron beam for suppression of microbunching instability, Phys. Rev. Accel. Beams **19**, 100701 (2016).
[26] M. Hüning and H. Schlarb, Measurement of the beam energy spread in the TTF photo-injector, in *Proceedings of the 20th Particle Accelerator Conference, Portland, Oregon, USA, 2003* (IEEE, Piscataway, NJ, 2003), p. 2074.
[27] C. Feng, T. Zhang, J. Chen, H. Deng, M. Zhang, X. Wang, B. Liu, T. Lan, D. Wang, and Z. Zhao, Measurement of the average local energy spread of electron beam via coherent harmonic generation, Phys. Rev. ST Accel. Beams **14**, 090701 (2011).
[28] S. Reiche, GENESIS 1.3: a fully 3D time-dependent FEL simulation code, Nucl. Instrum. Methods Phys. Res., Sect. A **429**, 243 (1999).
[29] R. Bonifacio, C. Pellegrini, and L. M. Narducci, Collective instabilities and high-gain regime in a free electron laser, Opt. Commun. **50**, 373 (1984).
[30] E. Prat, M. Calvi, R. Ganter, S. Reiche, T. Schietinger, and T. Schmidt, Undulator beamline optimization with integrated chicanes for X-ray free-electron-laser facilities, J. Synchrotron Radiat. **23**, 861 (2016).
[31] P. Emma, K. Bane, M. Cornacchia, Z. Huang, H. Schlarb, G. Stupakov, and D. Walz, Femtosecond and Subfemtosecond X-Ray Pulses from a Self-Amplified Spontaneous-Emission–Based Free-Electron Laser, Phys. Rev. Lett. **92**, 074801 (2004).
[32] E. Prat, M. Aiba, S. Bettoni, B. Beutner, S. Reiche, and T. Schietinger, Emittance measurements and minimization at the SwissFEL Injector Test Facility, Phys. Rev. ST Accel. Beams **17**, 104401 (2014).
[33] K. Floettmann, ASTRA User's Manual, 2000, http://www.desy.de/~mpyflo/.